Research article

Xiao Hu and Jian Wang*

Design of graphene-based polarization-insensitive optical modulator

Abstract: By exploiting the electroabsorption effect of graphene, we present a graphene-based polarization-insensitive optical modulator. The waveguide structure consists of a silica substrate, high-index silicon strip waveguide, Si_3N_4 dielectric spacer, two graphene layers, and two metal electrodes. The modulator performance is comprehensively studied in terms of attenuation, insertion loss, modulation depth, and bandwidth. We achieve broadband >16 dB attenuation graphene-based optical modulator over a 35 nm wavelength range (covering C band) with an imbalance of no >1 dB and insertion loss of <2 dB for transverse magnetic and transverse electric polarized modes. Moreover, the electrical properties such as energy per bit consumption (E_{bit}) are also studied.

Keywords: graphene; modulators; optical devices; waveguides.

1 Introduction

Optical modulator is one of the key components in optoelectronic integrated circuits, which converts electronic signals into high bit-rate photonic data. It is a device that can be used to modulate the properties of light such as its phase, amplitude, or polarization by electro-optic effect [1], electroabsorption (EA) effect [2], magneto-optic effect [3], and thermo-optic effect [4]. Traditional modulators are usually based on interference (Mach-Zehnder interferometers), resonance (ring resonators), and bandgap absorption (germanium-based EA modulators).

The early modulators employing lithium niobate waveguides [5] have advantages of stable operation over temperature, nearly zero-chirp, and bias-free. Although they have been extensively used in fiber-optic communication systems, the large footprint and low modulation efficiency might limit their further applications in optoelectronic integrated circuits. Later, a fully integrated silicon (Si) waveguide modulator based on Mach-Zehnder interferometer technology [6, 7], which is compatible with conventional complementary metal-oxide semiconductor (CMOS) processing, is reported. Then, a high-speed Si optical modulator using MOS capacitor is experimentally realized by Liu et al. [8] with modulation bandwidth exceeding 1 GHz. Through improvements in material quality, device design, and driver circuitry, an Si modulator with a bandwidth of 10 GHz was achieved by Liao et al. [9]. Significant progress also has been made for Mach-Zehnder modulators, with operation speed of up to 40–60 Gbit/s [10–14]. Recently, some impressive Si modulators based on microdisks, microrings, and photonic crystals exhibit the advantages of small size [15, 16], low modulation power [15, 17], and high modulation speed of up to 44–50 Gbit/s [18–20]. GeSi EA modulators [21–23] and surface plasmon polariton modulators [24–27] are also extensively investigated to improve the modulation efficiency and reduce the active device area. However, most of the above-mentioned modulators suffer from low modulation efficiency, large footprint, substantial temperature sensitivities, narrow operating bandwidth, and high insertion loss. To mitigate those limitations, a modulator with ultracompact device footprint, small insertion loss, low energy consumption, ultrafast response, high modulation speed, broad operation bandwidth, and acceptable thermal tolerance is highly desirable.

Graphene [28] features unique properties such as strong coupling with light, gate-variable optical conductivity, extraordinary thermal conductivity, and ultrahigh saturable absorption, which show great potential applications in optical modulators. In the last 2 years, an EA optical modulator based on single-layer graphene was first fabricated by Liu et al. [29], which had a modulation depth of 0.16 dB/μm and an overall length of 40 μm. It

*Corresponding author: Jian Wang, Wuhan National Laboratory for Optoelectronics, School of Optical and Electronic Information, Huazhong University of Science and Technology, Wuhan 430074, Hubei, China, e-mail: jwang@hust.edu.cn
Xiao Hu: Wuhan National Laboratory for Optoelectronics, School of Optical and Electronic Information, Huazhong University of Science and Technology, Wuhan 430074, Hubei, China

can modulate the total transmission just by applying different drive voltages between the graphene and waveguide. To enhance the interaction of light with graphene, a double-layer graphene optical modulator was designed and experimentally demonstrated [30]. The modulator possesses higher modulation depth, smaller footprint, and lower energy consumption. The graphene-based waveguide-integrated EA modulator has the benefits of high modulation efficiency, broadband, high-speed operation, ultrasmall size, and thermal stability. Up to date, a series of theoretical investigations and experimental demonstrations of graphene-based optical modulators have been extensively researched [31–40]. Most of the proposed configurations are polarization sensitive, as are conventional semiconductor-based electrooptical modulators [7, 41]. The polarization-sensitive modulator based on graphene is attributed to the differential attenuation of two polarization modes [42]. However, those polarization-sensitive modulators might have some limitations in real practical applications.

(1) For linearly polarized incident light that is widely used in fiber-optic communication systems, it is desired to adjust the incident light polarization state in line with the polarization-sensitive modulator. In this case, a polarization-maintaining fiber or polarization controller is always required, resulting in the increase of the transmitter complexity. (2) When the incident light is circularly or elliptically polarized, it can be decomposed into two orthogonal linearly polarized components. As a result, one component of polarized light cannot be modulated by the polarization-sensitive modulator. Then, the coupling losses from optical fiber to modulator might become large. Thereby, it is reasonable to design a modulator that can solve the imperfection of a polarization-sensitive modulator. A polarization-insensitive graphene-based EA optical modulator concept is presented by Ye et al. [43]. However, the control of the angle of the slanted Si stripe waveguide might have some challenge in a practical fabrication process. In this scenario, a laudable goal would be to explore the polarization-insensitive graphene-based optical modulator.

In this paper, we present an EA polarization-insensitive modulator based on graphene-Si waveguide. The chemical potential of graphene $\mu = 0$ eV is chosen as the "OFF" state point, and the point of $\mu = 0.48$ eV is regarded as the "ON" state. The performance of the designed graphene-based modulator is comprehensively evaluated, showing a 3 dB modulation depth with a 10.35-μm-long waveguide for transverse magnetic (TM) and transverse electric (TE) polarized modes. When the length of the graphene-based hybrid waveguide is set as

50 μm, the required voltage to switch the optical modulator from its minimum absorption to maximum modulation is assessed to be $\Delta V = 6.72$ V, corresponding to $E_{bit} = 2.98$ pJ/bit.

2 Gate-variable dielectric constant of graphene

One of the important properties of graphene is gate-variable optical conductivity [29], which enables the feasibility of a graphene-based modulator. The conductivity of graphene can be dynamically tuned by applying drive voltages that will change the carrier density of graphene and accordingly shift the Fermi level E_F (also chemical potential μ) of graphene. Here, graphene is treated as an anisotropic material because it is one atom thick and its π electrons cause electric conduction in its plane. The out-of-plane conductivity $\sigma_\perp$ can be different from the in-plane conductivity $\sigma_\parallel$. For the in-plane optical conductivity $\sigma_\parallel$ of graphene, an analytic expression derived within the random phase approximation [44] is used, which is

$$
\begin{aligned}
\sigma_\parallel = \sigma_{inter} + \sigma_{intra} &= \frac{i8\sigma_0}{\pi} \frac{E_{th}}{E_{ph} + iEs} \ln\left[2\cos\left(\frac{E_F}{2E_{th}}\right)\right] \\
&+ \sigma_0\left[\frac{1}{2} + \frac{1}{\pi}\tan^{-1}\left(\frac{E_{ph} - 2E_F}{2E_{th}}\right) - \frac{i}{2\pi}\ln\frac{(E_{ph} + 2E_F)^2}{(E_{ph} - 2E_F)^2 + 4E_{th}^2}\right]
\end{aligned}
$$

(1)

where $\sigma_0 = e^2 / 4\hbar$ is the universal conductivity of graphene (e is the elementary charge and $\hbar$ is the reduced Planck constant), $E_{th} = k_B T_e$ is thermal energy in eV (k_B is the Boltzmann constant and T_e is the carrier's effective temperature), E_F is the Fermi energy (that is chemical potential μ) of graphene in eV, $E_{ph} = hc/\lambda$ is photon energy in eV (h is the Planck constant), and $E_s = \hbar / \tau$ is scattering energy in eV for the scattering time τ.

The complex dielectric function $\varepsilon_\parallel(\mu)$ can be obtained from the complex optical conductivity of graphene written by

$$
\varepsilon_\parallel(\mu) = 2.5 + \frac{i\sigma(\mu)}{\omega\varepsilon_0\Delta}
$$

(2)

where $\Delta = 0.7$ nm is a thickness of the graphene layer, and ε_0 is the permittivity of vacuum, but the out-of plane permittivity is assumed to be $\varepsilon_\perp = 2.5$ [44].

The dielectric constant $\varepsilon_\parallel$ of graphene is calculated as a function of the chemical potential μ for a wavelength of $\lambda = 1550$ nm, $T_e = 300$ K, $\tau = 0.1$ ps, as shown in Figure 1A. Figure 1B shows the dielectric constant of graphene as a
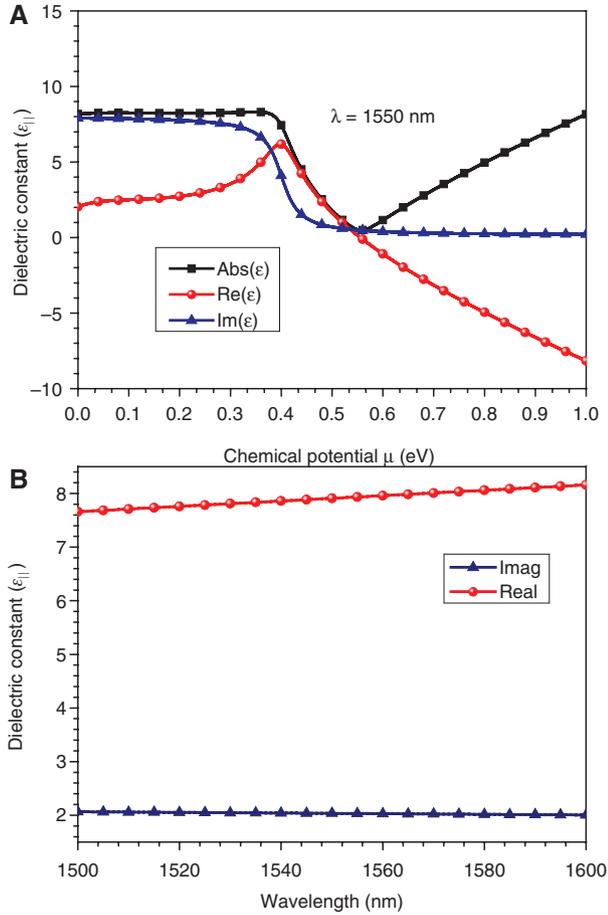
Figure 1: The dielectric constant of graphene as a function of chemical potential and incident light wavelength.
(A) Calculated dielectric constant of graphene (real part, imaginary part, and magnitude) as a function of chemical potential for $\lambda = 1550$ nm and (B) permittivity of graphene as a function of incident light wavelength under 0 eV chemical potential.

Figure 2: The structure of the polarization-insensitive optical modulator.
(A) Three-dimensional schematic illustration of the device and (B) cross-section of the hybrid Si waveguide. Inset: electric field distribution of TM and TE modes.

function of incident light wavelength when the chemical potential of graphene is 0 eV.

3 Concept and principles

Figure 2A and B shows the structure of the polarization-insensitive optical modulator. The proposed graphene-based polarization-insensitive optical modulator consists of a silica substrate, high-index Si strip waveguide, Si_3N_4 dielectric spacer, two graphene layers, and two metal electrodes. The two graphene flakes are extended out from opposite sides of the ridge Si waveguide for metallization. As graphene interacts with the tangential (in-plane) electric field of electromagnetic waves (Figure 2, inset), the interband transitions in graphene occurs. For TM and TE polarized modes, only the corresponding field component
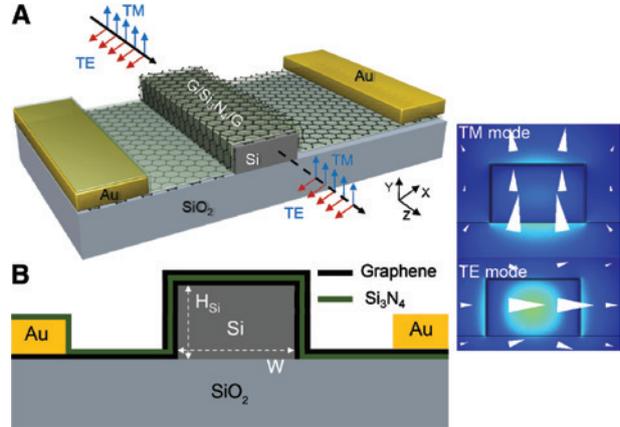
(horizontal and vertical polarization directions) has an effective interaction with graphene [45]. Therefore, the mode that presents the higher fraction of its field parallel to graphene, at the graphene position, experiences the higher absorption, which is response for the graphene-based polarization-sensitive modulator [29]. The polarization-dependent absorption is determined by the tangential (in-plane) electric field that overlaps with the graphene layer, and the waveguide design directly determines this fraction. Therefore, with a proper geometry structure of the Si waveguide, two graphene flakes can impose equal influence on TE and TM modes in the ridge waveguide.

The performance of the designed graphene-based polarization-insensitive modulator could be analyzed using capacitor models. The applied gate voltage changes the charge-carrier density in graphene, $n = \alpha(V_g + V_0)$, and shifts the Fermi level E_F (also chemical potential μ) as follows [29]:

$$\mu = \hbar V_F \sqrt{\pi \,|\, \alpha(V_g + V_0)\,|} \tag{3}$$

where n is the electron-hole doping concentration, $V_F = 0.9 \times 10^6$ m/s is the Fermi velocity [29], V_0 is the voltage offset caused by the natural doping, and V_g denotes the applied gate voltage. $\alpha = \dfrac{\varepsilon_0 \varepsilon_r}{de}$ is estimated using a simple parallel-plate capacitor, where ε_r together with ε_0 denotes the permittivity of the dielectric inside the capacitor, d is the distance between the capacitor plates, and e is the elementary charge. Consequently, the applied voltage V_g adjusts the chemical potential μ (E_F), the variation of which changes the complex optical conductivity σ, resulting in the tuning of the complex dielectric constant $\varepsilon_{\parallel}$.

4 Simulation results

In this work, the numerical simulations are performed based on the finite-element method. In the simulations, the boundary condition of the designed graphene-Si waveguide is set as a perfect matched layer. The thickness of the graphene layer is modeled as 0.7 nm.

Here, we first study the geometry dependence (Si waveguide width W) of the attenuation for TE and TM modes. Then, we define the insertion loss (minimum attenuation) and modulation depth (maximum attenuation-minimum attenuation) of graphene-based polarization-insensitive modulator. Finally, the attenuation as a function of the incident light wavelength is also evaluated.

To achieve polarization-independent modulation, different waveguide configurations are numerically analyzed with a double-layer graphene and dielectric spacer (Si_3N_4) placed on a strip Si waveguide (Figure 2). The thickness of the Si_3N_4 spacer is 7 nm. When setting Si waveguide height $H_{Si} = 250$ nm, we show the attenuation as a function of the Si waveguide width. Here, the chemical potential of graphene is set as $\mu = 0.3$ eV and the incident light wavelength is 1550 nm. As shown in Figure 3, we start our calculations with the width W varying from 300 to 430 nm. When the width of the Si waveguide is 300 nm, the attenuation of 0.248 and 0.543 dB/µm are calculated for the TM and TE polarized modes, respectively. Figure 3 also shows that the attenuation of TM mode increases with the width. However, as the width increases, the attenuation of TE mode decreases. When the Si waveguide width is about 407 nm, the attenuation curves of TM and TE polarized modes intersect (its value is 0.31 dB/µm), which imply that TM and TE polarized modes have the same loss.

Based on the results from the previous section, the detailed analysis will be performed for an Si waveguide with a width of 407 nm and a height of 250 nm. The change
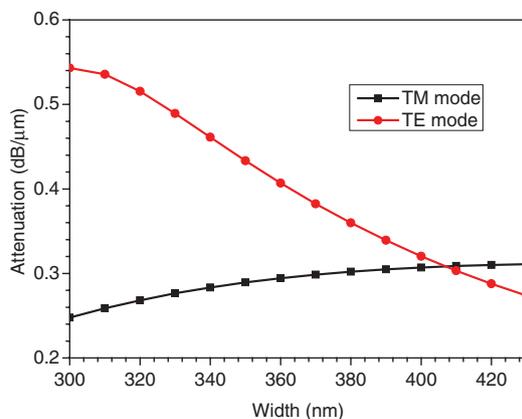
in attenuation and refractive index is analyzed as a function of the chemical potential for TM and TE polarized modes.

In Figure 1A, it is reminded that the complex dielectric constant of graphene can be tuned by changing the chemical potential of graphene through the applied drive gate voltage. The change of the complex dielectric constant of graphene affects the mode property (e.g. attenuation and effective refractive index N_{eff}). Figure 4A shows the attenuation of graphene-based polarization-insensitive waveguide modulator as a function of the chemical potential of graphene. Here, the working principle of the polarization-insensitive modulator relies on the EA effect of graphene. As shown in Figure 4A, the maximum attenuation is ~0.33 dB/µm with $\mu = 0$ eV for TE and TM mode. This chemical potential $\mu = 0$ eV point is chosen as the "OFF" state point. Considering the energy consumption of the designed modulator, we set $\mu = 0.48$ eV as the minimum attenuation chemical potential. The minimum attenuation is ~0.04 dB/µm (insertion loss). The point of $\mu = 0.48$ eV is regarded as the "ON" state. Therefore, the modulation depth is ~0.29 dB/µm (maximum attenuation-minimum attenuation). Hence, a ~10.35-µm-long

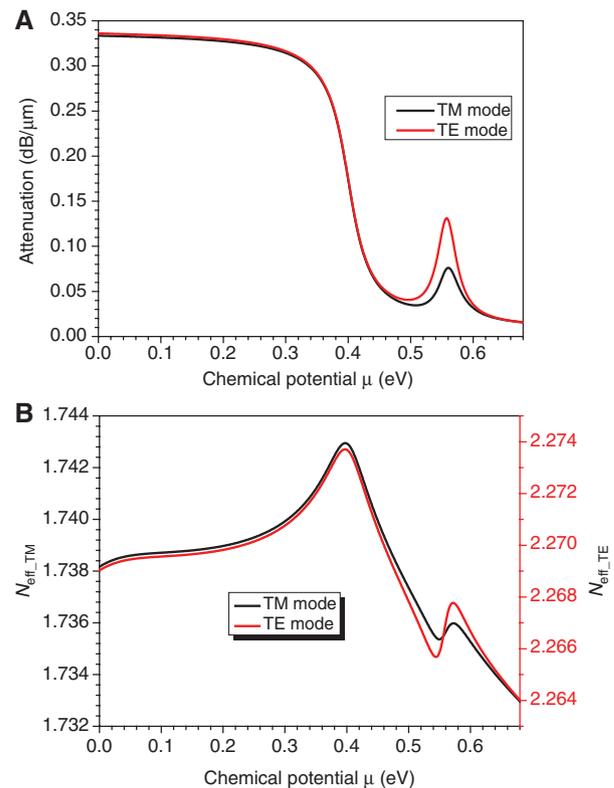Figure 3: Attenuation versus graphene-Si waveguide width.

Figure 4: The change of the complex dielectric constant of graphene affects the mode property.
(A) Attenuation and (B) mode effective index (N_{eff}) of the modulator as a function of chemical potential at $\lambda = 1551.7$ nm for two supported TM and TE polarized modes.

waveguide is required to achieve a 3 dB modulation depth for graphene-based polarization-insensitive optical modulator. Additionally, the same variation of the effective refractive index (N_{eff}) trend for TM and TE modes is also observed, as shown in Figure 4B. That is, the TE and TM modes have the same phase modulation when the chemical potential of graphene varies from 0 to 0.48 eV. The peak in Figure 4 at $\mu = 0.55$ eV may be caused by intraband absorption [31]. The variation of N_{eff} for TM and TE polarized modes is 4.7×10^{-3} when the chemical potential of graphene increases from 0 to 0.397 eV. Therefore, to introduce a π-phase shift between both arms of the graphene-based Mach-Zehnder interferometer, an active arm length of 164.894 μm is needed.

In addition to small footprint, low insertion loss, and high modulation depth, a large optical bandwidth is also expected for an ideal modulator. However, conventional electro-optic modulators based on integrated Si, germanium, and compound semiconductors suffer from a sophisticated design and an intrinsic relatively narrow optical bandwidth. Remarkably, the ultrahigh carrier mobility and strong optical absorption of graphene are independent of wavelength, which might enable a graphene-based modulator with a large optical bandwidth. To evaluate the optical bandwidth of the designed polarization-insensitive optical modulator, we study the attenuation as a function of the incident light wavelength covering the entire telecommunication C-band. Here, the length of graphene-based hybrid waveguide is set as 50 μm and the chemical potential of graphene is $\mu = 0$ eV "OFF" state. For the incident light wavelength of ~1551.7 nm, the attenuation is 16.44 dB for TM and TE polarized modes, as shown in Figure 5. We achieve a
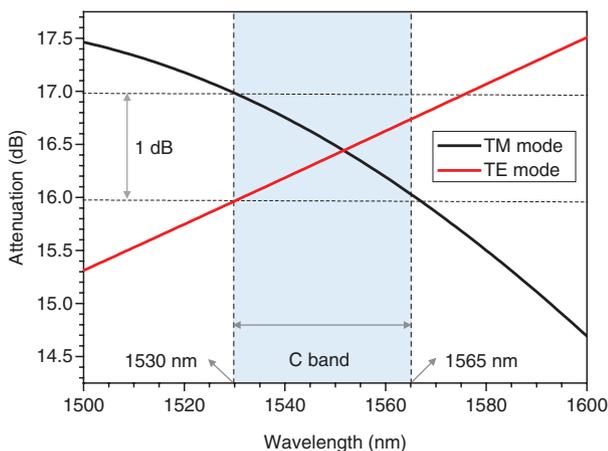
broadband >16 dB attenuation graphene-based polarization-insensitive optical modulator over a 35 nm wavelength range (covering C band) with an imbalance of no >1 dB and an insertion loss of <2 dB. The excellent properties fulfill the requirement of a broadband polarization-insensitive optical modulator.

5 Discussion

In addition to the metrics of optical modulators discussed above (insertion loss, modulation depth, and bandwidth), power consumption, the energy expended in producing each bit of data, has become particularly important for optical interconnects. Here, we study the electrical properties such as energy per bit consumption (E_{bit}) of the designed graphene-based polarization-insensitive optical modulator. Figure 6 shows the drive voltage of the modulator as a function of the chemical potential of graphene. The required voltage to switch the graphene-based polarization-insensitive optical modulator from its minimum absorption (0.48 eV, "ON" state) to its maximum modulation (0 eV, "OFF" state) is assessed to be $\Delta V = 6.72$ V, corresponding to $E_{bit} = 2.98$ pJ/bit. As we have mentioned above, the graphene-based modulator can also be used as a Mach-Zehnder interferometer, which is the key component of the I/Q modulator. The required voltage to introduce π-phase shift of the graphene-based Mach-Zehnder interferometer is 4.6 V (V_{π}), corresponding to $E_{bit} = 4.6$ pJ/bit.

Here, we estimate the 3 dB modulation bandwidth using an RC circuit model. With a carrier mobility exceeding a carrier mobility over 10^6 cm^2/(V s) at room temperature [46] and high saturation velocity of graphene, the

Figure 5: Attenuation of graphene-based polarization-insensitive optical modulator versus incident light wavelength for two supported TM and TE polarized modes.
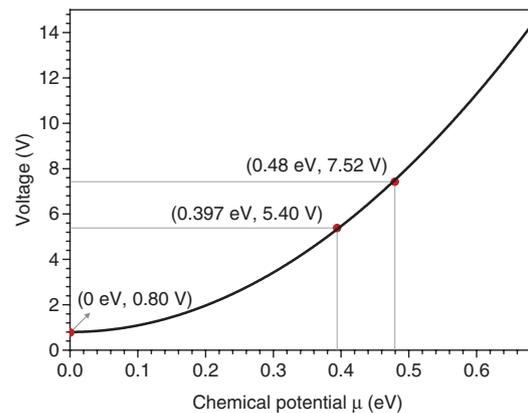

Figure 6: Drive voltage of the graphene-based polarization-insensitive optical modulator versus the chemical potential of graphene.

operation bandwidth of the device is not likely limited by the carrier transition time but the R_mC of the circuit, where R_m and C are the total series resistance and capacitance of the device, respectively. The total series resistance R_m is calculated by adding the ohmic resistances of the graphene layer as well as the resistance Rc of the metal contacts to the graphene layer; the former can be reduced to ~125 Ω/sq by highly doped, whereas the latter is several ohms [47]. The capacitance of the device can be calculated as $C = \varepsilon_0\varepsilon_d A_{gra}/d$, where ε_0, ε_d, A_{gra}, and d represent the permittivity of vacuum, the permittivity of the dielectric inside the capacitor, the area of graphene, the distance between the capacitor plates, and the charge of an electron, respectively. The capacitance of the structure is calculated to be $C = 2.64 \times 10^{-13}$ F. The 3 dB modulation bandwidth, $f_{3\,dB}$, is calculated by $f_{3\,dB} = 1/2\pi R_mC$ [33, 47, 48]. Hence, we calculate the bandwidth to be ~30.2 GHz by taking $R_m = ~20$ Ω [47, 48].

The estimated 3 dB modulation bandwidth based on the RC model is very similar to the Si modulator in Ref. [20]. Remarkably, the designed graphene-based optical modulator features broadband >16 dB attenuation over a 35 nm wavelength range (covering C band), small imbalance <1 dB, and low insertion loss <2 dB for the TM and TE polarized modes. Meanwhile, the area of graphene-based hybrid waveguide is only 0.407 × 50 μm and the required voltage to switch the optical modulator from its minimum absorption to maximum modulation is assessed to be $\Delta V = 6.72$ V. Moreover, the estimated 3 dB modulation bandwidth can be further improved by decreasing the capacitance of the structure. For applications not requiring 16 dB attenuation, one may reduce the waveguide length to further increase the 3 dB modulation bandwidth.

We present a theoretical treatment of waveguide-based graphene EA modulators, exploring its polarization dependence via finite-element simulations of optical mode overlaps with the graphene layer. By carefully choosing the width of the waveguide so that the TE and TM modes have equal absorption, covering the sidewalls of the waveguide with graphene and balancing the left/right sidewall overlap of the TM mode to equal the top/bottom surface overlap of the TE mode can be realized in a practical fabrication process [29, 30]. The possible fabrication process of the designed graphene-based polarization-insensitive optical modulator is as follows. The Si waveguide is fabricated using E-beam lithography combined with the inductively coupled plasma etching process. Chip-sized graphene sheet prepared on Cu film by chemical vapor deposition is protected by 200-nm-thick poly(methyl methacrylate) film. After the Cu film

is removed by the FeCl$_3$ solution, the graphene sheet is then rinsed and transferred on the fabricated waveguide. E-beam lithography is then used to define the active region, and oxygen plasma is applied to remove the undesired graphene on one side of the waveguide, leaving the other side for metallization. Thermal evaporation is used to deposit metal for electrode. The Si$_3$N$_4$ dielectric constant material is deposited on pristine graphene. Subsequently, similar patterning and etching procedures as the bottom graphene layer are performed to define the active tuning areas of graphene and top metal electrodes. Although the thickness of the Si$_3$N$_4$ spacer is 7 nm, the quantum capacitance of the designed modulator can be neglected [29]. In this work, the operation bandwidth is simulated using an equivalent circuit model with neglected Fermi-Dirac statistics, quantum capacitance effects, and random potential fluctuations in the graphene.

Here, the linearity of the graphene-based polarization-insensitive optical modulator is also evaluated. As shown in Figure 7, the attenuation and drive voltage have a nonlinear relationship within a wide range of drive voltage. The attenuation varies with the drive voltage when its value increases from 0.8 to 7.52 V. However, when choosing the drive voltage of the graphene modulator $V = 4.84$ V as the "OFF" state point and $V = 6.0$ V as the "ON" state point, the attenuation and drive voltage show an approximate linear relationship, as shown in the gray region in Figure 7.

In this work, by exploiting the EA effect of graphene, we present a graphene-based polarization-insensitive optical modulator. Besides, graphene can be widely used in lots of emerging applications. For instance, graphene can be employed as an optical nonlinear medium due to its ultrahigh third-order nonlinearity [49], which is corresponding to the Kerr nonlinearity, Re[$\chi^{(3)}$]. Note that
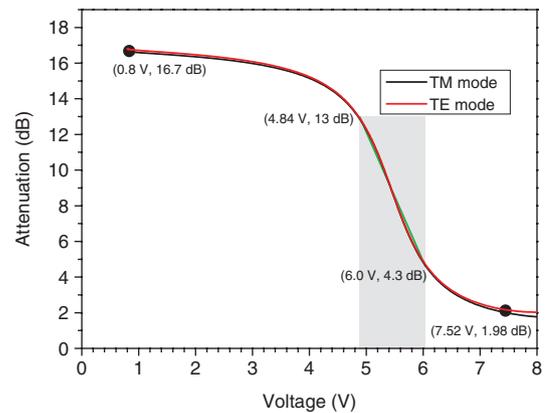

Figure 7: Attenuation of graphene-based polarization-insensitive optical modulator versus drive voltage.

optical nonlinearity can facilitate grooming optically efficient nonlinear signal processing applications [50]. The ultrahigh Kerr nonlinearity of graphene is a promising candidate for nonlinear optical signal processing [51]. Graphene-enhanced nonlinear optical signal processing has been widely demonstrated in various configurations, such as slow-light graphene-Si photonic crystal waveguide [52], fiber pigtail cross-section coated with a single-layer graphene [53–56], graphene based on microfiber [57], and graphene-assisted Si microring resonator [58, 59]. Benefiting from the linear and massless band structure of graphene [49], graphene-based optoelectronic devices are very fascinating.

6 Conclusions

In summary, we have proposed and designed a graphene-based polarization-insensitive optical modulator consisting of a silica substrate, high-index Si strip waveguide, Si_3N_4 dielectric spacer, two graphene layers, and two metal electrodes. The working principle of the graphene-based polarization-insensitive optical modulator relies on the EA effect of the graphene. We design the geometry of the Si waveguide that determines the tangential (in-plane) electric field that overlaps with the graphene layer to have the same loss for TM and TE polarized modes. In the graphene-based modulator, the applied drive voltage adjusts the chemical potential of graphene, the variation of which changes the complex optical conductivity, causing the variation of the complex dielectric constant and the resultant tuning of the mode properties. The chemical potential of graphene $\mu = 0$ eV is chosen as the "OFF" state point and the point of $\mu = 0.48$ eV is regarded as the "ON" state. A ~10.35-μm-long waveguide is required to achieve a 3 dB modulation depth for TM and TE polarized modes. A broadband >16 dB attenuation graphene-based polarization-insensitive optical modulator over a 35 nm wavelength range (covering C band) with an imbalance of no >1 dB and an insertion loss of <2 dB is achieved when the length of graphene-based hybrid waveguide is set as 50 μm and the chemical potential of graphene is $\mu = 0$ eV. We also study the electrical properties of the designed graphene-based modulator, such as E_{bit}, V_π, and bandwidth. The linearity is also evaluated for the designed graphene-based polarization-insensitive optical modulator.

References

[1] Soref R, Bennett B. Electrooptical effects in silicon. IEEE J Quantum Electron 1987;23:123–29.

[2] Reed GT, Mashanovich G, Gardes FY, Thomson DJ. Silicon optical modulators. Nat Photonics 2010;4:518–26.

[3] Ross WE, Psaltis D, Anderson RH. Two-dimensional magneto-optic spatial light modulator for signal processing. Opt Eng 1983;22:485–90.

[4] Cocorullo G, Iodice M, Rendina I. All-silicon Fabry-Perot modulator based on the thermo-optic effect. Opt Lett 1994;19:420–2.

[5] Wooten EL, Kissa KM, Yi-Yan A, et al. A review of lithium niobate modulators for fiber-optic communications systems. IEEE J Sel Top Quantum Electron 2000;6:69–82.

[6] Dainesi P, Chabloz M, Lagos A, Flückiger P. CMOS compatible fully integrated Mach-Zehnder interferometer in SOI technology. IEEE Photon Technol Lett 2000;12:660–2.

[7] Xu K, Snyman LW, Aharoni H. Si light-emitting device in integrated photonic CMOS ICs. Opt Mater 2017;69: 274–82.

[8] Liu A, Jones R, Liao L, et al. A high-speed silicon optical modulator based on a metal-oxide semiconductor capacitor. Nature 2004;427:613–5.

[9] Liao L, Samara-Rubio D, Morse M, et al. High speed silicon Mach-Zehnder modulator. Opt Express 2005;13:3129–35.

[10] Xiao X, Xu H, Li X, Li Z, Yu J. High-speed, low-loss silicon Mach-Zehnder modulators with doping optimization. Opt Express 2013;21:4116–25.

[11] Dong P, Chen L, Chen Y. High-speed low-voltage single-drive push-pull silicon Mach-Zehnder modulators. Opt Express 2012;20:6163–9.

[12] Thomson DJ, Gardes FY, Fedelim JM. 50-Gb/s silicon optical modulator. IEEE Photon Technol Lett 2012;24:234–6.

[13] Streshinsky M, Ding R, Liu Y. Low power 50 Gb/s silicon traveling wave Mach-Zehnder modulator near 1300 nm. Opt Express 2013;21:30350–7.

[14] Xiao X, Xu H, Li X, Li Z, Yu J. 60 Gbit/s silicon modulators with enhanced electro-optical efficiency. In: Optical Fiber Communication Conference. Optical Society of America, 2013: OW4J.3.

[15] Debnath K, O'Faolain LY, Gardes F, Steffan AG, Reed GT, Krauss TF. Cascaded modulator architecture for WDM applications. Opt Express 2012;20:27420–8.

[16] Watts MR, Zortman WA, Trotter DC, Young RW, Lentine AL. Vertical junction silicon microdisk modulators and switches. Opt Express 2011;19:21989–2003.

[17] Zortman WA, Lentine AL, Trotter DC, Watts MR. Low-voltage differentially-signaled modulators. Opt Express 2011;19:26017–26.

[18] Xiao X, Li X, Xu H, et al. 44-Gbit/s silicon microring modulators based on zigzag PN junctions. IEEE Photon Technol Lett 2012;24:1712–4.

[19] Baba T, Akiyama S, Imai M. 50-Gb/s ring-resonator-based silicon modulator. Opt Express 2013;21:11869–76.

[20] Xu K. Integrated silicon directly modulated light source using p-well in standard CMOS technology. IEEE Sens J 2016;16:6184–91.

[21] Liu J, Beals M, Pomerene A. Waveguide-integrated, ultralow-energy GeSi electro-absorption modulators. Nat Photonics 2008;2:433–7.

[22] Feng D, Liao S, Liang H. High speed GeSi electro-absorption modulator at 1550 nm wavelength on SOI waveguide. Opt Express 2012;20:22224–32.

[23] Feng D, Qian W, Liang H. High-speed GeSi electro-absorption modulator on the SOI waveguide platform. IEEE J Sel Top Quantum Electron 2013;19:64–73.

[24] Melikyan A, Lindenmann N, Walheim S. Surface plasmon polariton absorption modulator. Opt Express 2011;19:8855–69.

[25] Sorger VJ, Lanzillotti-Kimura ND, Ma RM. Ultra-compact silicon nanophotonic modulator with broadband response. Nanophotonics 2012;1:17–22.

[26] Lu Z, Zhao W, Shi K. Ultracompact electroa-bsorption modulators based on tunable epsilon-near-zero-slot waveguides. IEEE Photonics J 2012;4:735–40.

[27] Melikyan A, Alloatti L, Schindler PC, Li J, Leuthold J. High-speed plasmonic phase modulators. Nat Photonics 2014;8:229–33.

[28] Geim AK, Novoselov KS. The rise of graphene. Nat Mater 2007;6:183–91.

[29] Liu M, Yin X, Ulin-Avila E, Geng B, Zentgraf T, Zhang X. A graphene-based broadband optical modulator. Nature 2011;474:64–7.

[30] Liu M, Yin X, Zhang X. Double-layer graphene optical modulator. Nano Lett 2012;12:1482–5.

[31] Lu Z, Zhao W. Nanoscale electro-optic modulators based on graphene-slot waveguides. J Opt Soc Am B 2012;29:1490–6.

[32] Yang L, Hu T, Hao R, et al. Low-chirp high-extinction-ratio modulator based on graphene-silicon waveguide. Opt Lett 2013;38:2512–5.

[33] Koester SJ, Li M. High-speed waveguide-coupled graphene-on-graphene optical modulators. Appl Phys Lett 2012;100:171107.

[34] Gosciniak J, Tan DT. Theoretical investigation of graphene-based photonic modulators. Sci Rep 2013;3:1897.

[35] Xu A, Jin Y, Yang L, Yang J, Jiang X. Characteristics of electro-refractive modulating based on graphene-oxide-silicon waveguide. Opt Express 2012;20:1–8.

[36] Sensale-Rodriguez B, Yan R, Zhu M. Efficient terahertz electro-absorption modulation employing graphene plasmonic structures. Appl Phys Lett 2012;101:261115.

[37] Sensale-Rodriguez B, Yan R, Kelly MM. Broadband graphene terahertz modulators enabled by intraband transitions. Nat Commun 2012;3:780.

[38] Phare AT, Lee YHD, Cardenas J, Lipson M. Graphene electro-optic modulator with 30 GHz bandwidth. Nat Photonics 2015;9:511–4.

[39] Youngblood N, Anugrah Y, Ma RJ, Koester S, Li M. Multifunctional graphene optical modulator and photo-detector integrated on silicon waveguides. Nano Lett 2014;14:2741–6.

[40] Dalir H, Xia Y, Wang Y, Zhang X. Athermal broadband graphene optical modulator with 35 GHz speed. ACS Photonics 2016;3:1564–8.

[41] Soref RA. Electro-optical and nonlinear optical coefficients of ordered group IV semiconductor alloys. J Appl Phys 1992;72:626–30.

[42] Bao Q, Zhang H, Wang B, et al. Broadband graphene polarizer. Nat Photonics 2011;5:411–5.

[43] Ye SW, Liang D, Lu RG, et al. Polarization-independent modulator by partly tilted graphene-induced electro-absorption effect. IEEE Photon Technol Lett 2017;29:23–6.

[44] Kwon MS. Discussion of the epsilon-near-zero effect of graphene in a horizontal slot waveguide. IEEE Photonics J 2014;6:1–9.

[45] de Oliveira REP, de Matos CJS. Graphene based waveguide polarizers: in-depth physical analysis and relevant parameters. Sci Rep 2015;5:1–8.

[46] Baringhaus J, Ruan M, Edler F, et al. Exceptional ballistic transport in epitaxial graphene nanoribbons. Nature 2014;506:349–54.

[47] Qiu C, Gao W, Vajta RI, Ajayan PM, Kono J, Xu Q. Efficient modulation of 1.55 μm radiation with gated graphene on a silicon microring resonator. Nano Lett 2014;14:6811–5.

[48] Hu X, Wang J. High-speed gate-tunable terahertz coherent perfect absorption using a split-ring graphene. Opt Lett 2015;40:5538–41.

[49] Hendry E, Hale PJ, Moger J, Savchenko AK, Mikhailov SA. Coherent nonlinear optical response of graphene. Phys Rev Lett 2010;105:097401.

[50] Willner AE, Yilmaz OF, Wang J, et al. Optically efficient nonlinear signal processing. IEEE J Sel Top Quantum Electron 2011;17:320–32.

[51] Wang J, Hu X. Recent advances in graphene-assisted nonlinear optical signal processing. J Nanotechnol 2016;2016:1–18.

[52] Gu T, Petrone N, McMillan JF, et al. Regenerative oscillation and four-wave mixing in graphene optoelectronics. Nat Photonics 2012;6:554–9.

[53] Hu X, Zeng M, Wang A, Zhu L, Fu L, Wang J. Graphene-assisted nonlinear optical device for four-wave mixing based tunable wavelength conversion of QPSK signal. Opt Express 2015;23:26158–67.

[54] Wang A, Hu X, Zhu L, Zeng M, Fu L, Wang J. Experimental demonstration on two-input optical high-base hybrid doubling and subtraction functions in graphene. Opt Express 2015;23:31728–35.

[55] Hu X, Zeng M, Long Y, et al. Phase conjugated and transparent wavelength conversions of Nyquist 16-QAM signals employing a single-layer graphene coated fiber device. Sci Rep 2016;6:22379.

[56] Hu X, Wang A, Zeng M, et al. Graphene-assisted multiple-input high-base optical computing. Sci Rep 2016;6:32911.

[57] Wu Y, Yao B, Cheng Y, et al. Four-wave mixing in a microfiber attached onto a graphene film. IEEE Photonics Technol Lett 2014;26:249–52.

[58] Hu X, Long Y, Ji M, et al. Graphene-silicon microring resonator enhanced all-optical up and down wavelength conversion of QPSK signal. Opt Express 2016;24:7168–77.

[59] Long Y, Wang Y, Hu X, et al. Channel-selective wavelength conversion of quadrature amplitude modulation signal using a graphene-assisted silicon microring resonator. Opt Lett 2017;42:799–802.